Supporting information
Similar ligand–metal bonding for transition metals and actinides? $5f^1$ $U(C_7H_7)_2^-$ versus $3d^n$ metallocenes

Dumitru-Claudiu Sergentu, Frédéric Gendron and Jochen Autschbach*

Department of Chemistry, University at Buffalo,
State University of New York, Buffalo, NY 14260-3000, USA

email: jochena@buffalo.edu

April 26, 2018

S1 Structures of the metallocenes

Experimental geometries for the studied TM metallocenes are available from both gas phase electron diffraction[1–4] and condensed phase X-ray diffraction (XRD).[5–8] A single crystal XRD structure is available for the $5f^1$ $U(C_7H_7)_2^-$.[9] As it is well known, global minimum structures of metallocenes, i.e. eclipsed or staggered, cannot be unequivocally established due to low ring-rotation energy barriers. Recorded average structures show nearly D_5 symmetry and, usually, eclipsed conformations for the metallocenes in the gas phase but staggered conformations for the TM metallocenes and the $5f^1$ $U(C_7H_7)_2^-$ in the condensed phase, in agreement with computational predictions.[10–19] Optimized structural data are provided down below (Tables S1, S2) alongside available experimental structural parameters. The optimized structures are in good agreement with the experimental and previous computational data.

The ground state geometries of vanadocene and nickelocene feature a five-fold rotational axis of symmetry with a V^{II+} ($3d^3$) and a Ni^{II+} ($3d^8$) metal center respectively. The 3d orbital degeneracy is lifted by the axial LF, giving rise to a spin quartet $(3d_\sigma)^1(3d_\delta)^2(3d_\pi)^0$, and to a spin triplet $(3d_\sigma)^2(3d_\delta)^4(3d_\pi)^2$, electronic GS for vanadocene and nickelocene, respectively. The eclipsed conformers have D_{5h} symmetry and the optimized GSs belong to the ${}^4A_1'$, and ${}^3A_1'$ irreducible representations (irreps) for V and Ni, respectively, while the staggered conformers have D_{5d} symmetry and the GSs belong to the ${}^4A_{1g}$ and ${}^3A_{1g}$ irreps. Cobaltocene affords a $3d^7$ Co^{II+} ion. In the axial LF, the 3d degeneracy is split into a $3d_\sigma$ (a_1' or a_{1g} in $D_{5h/d}$) and twofold degenerate $3d_\delta$ (e_2' or

e_{2g}) and $3d_\pi$ (e''_1 or e_{1g}) orbitals. The unpaired electron in the degenerate $3d_\pi$ orbitals leads to an orbitally degenerate spin-doublet GS ($^2E''_1$ or $^2E_{1g}$). Jahn-Teller distortions[20,21] remove the orbital-degeneracy by symmetry lowering from $D_{5h/d}$ to $C_{2v/h}$, causing slightly puckered arene ligands. The lowest energy structure is the C_{2v} one, with a GS of $^2B_1$ symmetry.[14]

S2 Choice of active spaces and state-average schemes

Initial CAS calculations for the TM systems were performed using active spaces comprising the metal 3d shells and their electrons, *i.e.* CASSCF(3, 5), (7, 5) and (8, 5) for the $TM(C_5H_5)_2$, TM = V, Co and Ni respectively. In order to account for double-shell correlation,[22] a set of five 3d′ orbitals was added to the active spaces of $Co(C_5H_5)_2$ and $Ni(C_5H_5)_2$ leading to (7, 10) and (8, 10) active spaces. Note that the 3d′-shell correlation is not significant in $V(C_5H_5)_2$.[15,23] Lastly, the two $3d_\pi$-based bonding MOs were added to the active spaces leading to (7, 7), (11, 12) and (12, 12) calculations for $V(C_5H_5)_2$, $Co(C_5H_5)_2$ and $Ni(C_5H_5)_2$ respectively. The latter active spaces were finally selected as detailed in Section S3 (see below). The state-average was performed over i) 10 spin-quartet, ii) 40 spin-doublet and 10 spin-quartet, and iii) 21 spin-triplet and 28 spin-singlet states for $V(C_5H_5)_2$, $Co(C_5H_5)_2$ and $Ni(C_5H_5)_2$ respectively.

For the $5f^1$ $U(C_7H_7)_2^-$, calculations were performed with a minimal active space in which one electron spanned the seven 5f orbitals, *i.e.* CASSCF(1, 7). Then, the $6d_\delta$- and $5f_\delta$-based bonding and antibonding MOs were successively added to the active space. With the bonding $5f_\delta$-based MOs the active space is (5, 9). Adding further the bonding and antibonding $6d_\delta$-based MOs leads to a (9, 13) active space. Finally, the addition of the $6d_\sigma$-based nonbonding MO and of the $6d_\pi$-based antibonding MOs, a (9, 16) active space is obtained. The state average was performed over seven SR spin-doublet states. Only the results obatined with CAS(9, 13) are reported in the main manuscript since this active space is well balanced (includes all important bonding and corresponding antibonding MOs), describing at best the bonding in $U(C_7H_7)_2^-$. Results obtained with the remaing active spaces are reported in the SI and adequately referenced in the main manuscript.

Spin polarization effects were introduced through the RASCI(n_{el}, [RAS1, RAS2, RAS3]) approach for the TM = V, Co metallocenes and for the $5f^1$ $U(C_7H_7)_2^-$. A large active space is divided in three sub-spaces (RAS1, RAS2 and RAS3), and then multiconfigurational wave functions are generated by correlating n_{el} electrons among the different sub-spaces, with the restrictions that only n holes are allowed in RAS1 and only m electrons in RAS3 ($n = m = 1$ was chosen in this work). For the TM cases, from the CAS-SR converged MOs (largest CAS), only the magnetic orbitals are kept in RAS2, the remaining π MOs (below the magnetic orbitals) were added in RAS1 alongside additional 14 C $2p_\sigma$ orbitals for TM = Co, and additional 10 C 1s orbitals for TM = V, while a large set of 100 virtual orbitals were added in RAS3. For the $5f^1$ $U(C_7H_7)_2^-$, the $5f_\sigma$ and

$5f_\pi$ MOs from the converged CAS(9, 16) set are kept in RAS2. Then, the $(\pi_\delta - 5f_\delta)_+$, $(\pi_\delta - 6d_\delta)_+$ and remaining valence π MOs are added to RAS1 (9 MOs in total) alongside an additional 14 C $2p_\sigma$ orbitals, while 100 virtual orbitals are added to RAS3.

S3 Choosing the active space for the TM metallocenes

For metallocenes, accurate energetics has proved to be difficult to predict through CAS approaches with issues being related to the manifestation of strong dynamic correlation, difficult to capture within affordable active spaces.[15,23,24] In this work, both the 3d (*e.g.* $3d_\sigma$, $(\pi_\delta - 3d_\delta)_+$ and $(\pi_\pi - 3d_\pi)_-$ MOs) and $3d + 3d'$ active spaces were found unsuitable to tackle the low-lying electronic structure of cobaltocene in particular, since they yielded an incorrect spin-quartet GS in CAS-SR calculations. This scenario is common to an uncomplexed Co^0 atom. That is, a large fraction of dynamic correlation is not captured within the small active spaces and the inclusion of additional orbitals alongside the 3d and 3d′ sets is necessary to obtain a correct ordering of the electronic states at the CAS-SR level. The active space of cobaltocene, and of the other metallocenes, were therefore extended with the bonding $(\pi_\pi - 3d_\pi)_+$ MOs. With the resulted active spaces, CAS-SR and PT2-SR ground-state potential energy surface (PES) scans were performed along the distances between the metal centers and ring-centroids, in order to check if they reproduce acceptable equilibrium r^{ring} values in the different metallocenes (see scans in Figure S2). PT2-SR predicted r^{ring} values (1.87, 1.67 and 1.77 Å for vanadocene, cobaltocene and nickelocene respectively) which are at least 0.15 Å shorter than the CAS-SR counterparts, and systematically shorter than the measured or DFT-GGA ones by 0.04 Å on average. This is due to the selected active spaces which include the bonding $(\pi_\delta - 3d_\delta)_+$ MOs but not their antibonding pairs, and thus bonding is slightly favoured. Nonetheless, the obtained values are accurate enough to state that the bonding in these metallocenes is, to a good extent, captured by the selected larger active spaces.

S4 $U(C_7H_7)_2^-$: Orbital composition of the GS SOC wavefunction based on CF arguments

The expansion of key $|J, \pm M_J\rangle$ Kramers of the $5f^1$ U^V ion, in terms of the $f_\sigma, f_\pi, f_\delta, f_\phi$ SOC free states, are:[25,26]

$$|\frac{5}{2}, \pm\frac{1}{2}\rangle = 0.655f_\sigma + 0.756f_\pi \quad (1)$$

$$|\frac{5}{2}, \pm\frac{5}{2}\rangle = 0.377f_\delta + 0.926f_\phi \quad (2)$$

$$|\frac{7}{2},\pm\frac{1}{2}\rangle = 0.756\mathrm{f}_{\sigma} + 0.655\mathrm{f}_{\pi} \tag{3}$$

Gourier *et al.* found that the expression of the $|J,\pm M_J\rangle$ GS wavefunction according to which the experimental g factors are well reproduced, is a mixture of the $|\frac{5}{2},\pm\frac{1}{2}\rangle$ and $|\frac{5}{2},\pm\frac{5}{2}\rangle$ Kramers states:[25]

$$|\pm\rangle = \pm 0.948|\frac{5}{2},\pm\frac{1}{2}\rangle \pm 0.323|\frac{5}{2},\pm\frac{5}{2}\rangle \tag{4}$$

Combining eqs. (1), (2) and (4), the $|J,\pm M_J\rangle$ GS wavefunction expression reads:[25]

$$|\pm\rangle = \mp 0.621\mathrm{f}_{\sigma} \pm 0.717\mathrm{f}_{\pi} \mp 0.122\mathrm{f}_{\delta} \pm 0.298\mathrm{f}_{\phi} \tag{5}$$

which in terms of percentage composition reads:[25]

$$|\pm\rangle = 38.5\%\mathrm{f}_{\sigma} + 51.4\%\mathrm{f}_{\pi} + 1.5\%\mathrm{f}_{\delta} + 8.9\%\mathrm{f}_{\phi} \tag{6}$$

S5 Spin density distribution in $U(C_7H_7)_2^-$ vs. $U(C_8H_8)$

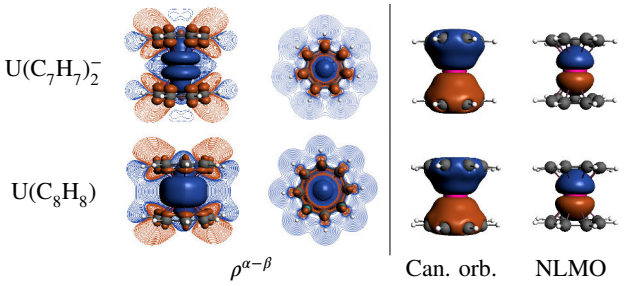

Figure S1: $5f^1$ vs. the $5f^2$ actinocene. Left: GS Spin density distribution ($\rho^{\alpha-\beta}$) visualized with an isosurface value of ± 0.001. Contour-line plots show the spin polarization in the vertical plane, containing the seven/eight-fold rotational axis, and in the horizontal plane defined by the C atoms of an arene ligand. Right: The U $6p_z$-based canonical orbital (can. orb.) and corresponding natural localized MO (NLMO), vizualized with an isosurface value of ± 0.02. For the $\rho^{\alpha-\beta}$ plots, orange (light shading) and blue (dark shading) stand for negative and positive spin density respectively. BP/TZ2P calculations on the eclipsed experimental structures.

The $U(C_8H_8)$ system affords essentially a $5f^1_{\pi}5f^1_{\phi}$ ($^3E_{2g}$ in D_{8h}) GS[27–29] for which AOC BP/TZ2P calculations, followed by an NBO analysis, reveals ligand atomic spin populations similar with those in $U(C_7H_7)_2^-$ (see Table S3). This aspect is evident also from the comparison of the spin density distribution in the $5f^1$ vs. the $5f^2$ actinocene visualized in Figure S1. The figure further shows plots of the U $6p_z$-based canonical and corresponding natural localized MO. While, as expected, the canonical orbital appears largely delocalized, in fact overlapping with arene σ bonds alike the $3d_{\sigma}$ localized orbital in $V(C_5H_5)_2$, the natural orbital is strongly localized on the U center

is strongly core-like in character (100% U $6p_z$ character in both actinocenes). We conclude that a spin polarization of the arene ligands in the $5f^1$ or the $5f^2$ actinocene by the U 6p or 6s electrons (the $6p_x$, $6p_y$ and 6s natural localized orbitals have the same features as the $6p_z$ natural orbital and therefore not shown in Figure S1) is unlikely to be effective. In fact, in $U(C_7H_7)_2^-$, a polarization of the ligand σ networks would more likely arise from the U $6d_\sigma$ orbital. However, the total population of $6d_\sigma$ is around 0.1 (Table S5), and thus it would also be an unlikely source for such a spin-polarization.

Table S1: Equilibrium bond lengths (in Å) between the metal centers and i) ring centroids (r^{ring}), and ii) C atoms (r^{C}), and between pairs of C atoms ($r^{\text{C-C}}$), at eclipsed and staggered conformers. Top-bar notation is used to denote an averaged distance.

System	Functional	Eclipsed			Staggered			Jahn-Teller	
		r^{ring}	r^{C}	$r^{\text{C-C}}$	r^{ring}	r^{C}	$r^{\text{C-C}}$	$\bar{r}^{\text{C}}$	$\bar{r}^{\text{C-C}}$
$Co(C_5H_5)_2$	BP	1.72	2.11	1.43	1.73	2.11	1.43	2.10	1.43
	PBE	1.71	2.10	1.43	1.72	2.10	1.43	2.10	1.43
	B3LYP	1.78	2.15	1.42	1.79	2.16	1.42	2.15	1.42
	PBE0	1.73	2.11	1.42	1.74	2.12	1.42	2.11	1.42
	Expt.[a]	1.74	-	-	1.74	-	-	2.12	1.43
$U(C_7H_7)_2^-$	BP	2.02	2.60	1.42	2.02	2.60	1.42	-	-
	PBE	2.01	2.59	1.42	2.01	2.59	1.42	-	-
	B3LYP	2.04	2.62	1.42	2.05	2.62	1.42	-	-
	PBE0	1.99	2.58	1.42	2.00	2.58	1.42	-	-
	Expt.[b]	1.98	2.53	1.37	1.98	2.53	1.37	-	-

[a]Gas phase electron diffraction data.[1,2] [b]XRD data.[9]

Table S2: Calculated equilibrium bond lengths (in Å) between the metal centers and i) ring centroids (r^{ring}), and ii) ring C atoms (r^{C}), and between pairs of C atoms ($r^{\text{C-C}}$), at the eclipsed and staggered conformers.

System	Functional	Eclipsed			Staggered		
		r^{ring}	r^{C}	$r^{\text{C-C}}$	r^{ring}	r^{C}	$r^{\text{C-C}}$
$V(C_5H_5)_2$	BP	1.92	2.27	1.43	1.93	2.28	1.43
	PBE	1.91	2.26	1.43	1.92	2.27	1.43
	B3LYP	1.97	2.31	1.42	1.98	2.31	1.42
	PBE0	1.93	2.27	1.41	1.93	2.27	1.41
	Expt.[a]	1.93	2.28	1.43	1.93	2.28	1.43
$Ni(C_5H_5)_2$	BP	1.82	2.19	1.43	1.82	2.19	1.43
	PBE	1.81	2.18	1.43	1.81	2.18	1.43
	B3LYP	1.87	2.23	1.42	1.87	2.23	1.42
	PBE0	1.83	2.19	1.42	1.83	2.19	1.42
	Expt.[b]	1.83	2.20	1.43	1.83	2.20	1.43

[a]Gas phase electron diffraction data.[3] [b]Gas phase electron diffraction data.[4]

Table S3: Atomic spin populations obtained with various functionals and TZ2P basis sets.[a]

System	Atom	BP		PBE	B3LYP	PBE0	
		MPA	NPA	MPA	MPA	MPA	NPA
$Co(C_5H_5)_2$[b]	Co	0.728	0.664	0.723	*1.082*	*1.112*	*1.039*
		0.718	0.657	0.715	0.865	0.868	0.810
	C	0.028	0.034	0.028	*−0.009*	*−0.013*	*−0.004*
		0.029	0.035	0.029	0.013	0.013	0.020
	H	−0.001	−0.001	0.000	*0.001*	*0.002*	*0.000*
		−0.001	−0.001	0.000	0.000	0.000	−0.001
$U(C_7H_7)_2^-$[c]	U	1.299	1.230	1.282	1.521	1.530	1.457
		1.214	1.171	1.233	1.368	1.452	1.381
	C	−0.025	−0.019	−0.024	−0.039	−0.040	−0.035
		−0.023	−0.016	−0.021	−0.029	−0.035	−0.030
	H	0.004	0.003	0.004	0.002	0.003	0.002
		0.005	0.004	0.004	0.002	0.003	0.003
$U(C_8H_8)$[d]	U	2.192	2.141				
	C	−0.014	−0.010				
	H	0.002	0.001				

[a]Italic font is used to emphasize that the converged DFT solution is significantly spin-contaminated. For the eclipsed cobaltocene, $\langle \hat{S}^2 \rangle \simeq 0.94$ instead of 0.75. [b](Averaged) atomic spin populations obtained at the optimized D_{5h}/Jahn-Teller C_{2v} geometry are listed on the first/second lines. [c]Atomic spin populations obtained at the optimized/experimental D_{7h} geometry are listed on the first/second lines. [d]The experimental D_{8h} geometry with standard C–H bond lengths, is used.[30,31]

Table S4: Atomic spin populations obtained with various functionals and TZ2P basis sets.

System	Atom	BP		PBE	B3LYP	PBE0	
		MPA	NPA	MPA	MPA	MPA	NPA
$V(C_5H_5)_2$[a]	V	3.030	2.859	2.988	3.018	3.057	2.922
	C	−0.005	0.011	−0.001	−0.005	−0.009	0.005
	H	0.002	0.003	0.002	0.003	0.004	0.003
$Ni(C_5H_5)_2$[a]	Ni	1.050	1.001	1.062	1.212	1.240	1.235
	C	0.101	0.103	0.098	0.081	0.079	0.079
	H	−0.005	−0.003	−0.004	−0.002	−0.003	−0.003

[a]The optimized D_{5h} geometries are used.

Table S5: Calculated metal electronic configuration in cobaltocene and $U(C_7H_7)_2^-$.[a]

System	Spin	Configuration
$Co(C_5H_5)_2$[b]	α	$(3d_\sigma)^{0.98}(3d_\pi)^{1.58}(3d_\delta)^{1.87}$
	β	$(3d_\sigma)^{0.98}(3d_\pi)^{0.95}(3d_\delta)^{1.84}$
$U(C_7H_7)_2^-$[b]	α	$(5f_\sigma)^{0.94}(5f_\pi)^{0.15}(5f_\delta)^{1.08}(5f_\phi)^{0.02}(6d_\sigma)^{0.06}(6d_\pi)^{0.37}(6d_\delta)^{0.63}$
	β	$(5f_\sigma)^{0.04}(5f_\pi)^{0.15}(5f_\delta)^{0.85}(5f_\phi)^{0.02}(6d_\sigma)^{0.06}(6d_\pi)^{0.35}(6d_\delta)^{0.61}$
$U(C_7H_7)_2^-$[c]	α	$(5f_\sigma)^{0.93}(5f_\pi)^{0.17}(5f_\delta)^{1.06}(5f_\phi)^{0.02}(6d_\sigma)^{0.07}(6d_\pi)^{0.36}(6d_\delta)^{0.65}$
	β	$(5f_\sigma)^{0.04}(5f_\pi)^{0.16}(5f_\delta)^{0.86}(5f_\phi)^{0.02}(6d_\sigma)^{0.07}(6d_\pi)^{0.35}(6d_\delta)^{0.63}$
$U(C_7H_7)_2^-$[d]	α	$(5f_\sigma)^{0.93}(5f_\pi)^{0.14}(5f_\delta)^{1.08}(5f_\phi)^{0.02}(6d_\sigma)^{0.07}(6d_\pi)^{0.38}(6d_\delta)^{0.68}$
	β	$(5f_\sigma)^{0.04}(5f_\pi)^{0.14}(5f_\delta)^{0.73}(5f_\phi)^{0.02}(6d_\sigma)^{0.06}(6d_\pi)^{0.36}(6d_\delta)^{0.64}$
$U(C_8H_8)$[c]	α	$(5f_\sigma)^{0.96}(5f_\pi)^{0.12}(5f_\delta)^{0.75}(5f_\phi)^{0.90}(6d_\sigma)^{0.06}(6d_\pi)^{0.35}(6d_\delta)^{0.50}$
	β	$(5f_\sigma)^{0.05}(5f_\pi)^{0.11}(5f_\delta)^{0.54}(5f_\phi)^{0.02}(6d_\sigma)^{0.06}(6d_\pi)^{0.33}(6d_\delta)^{0.45}$

[a]Natural population analyses, BP/TZ2P. [b]Optimized eclipsed geometry. [c]Experimental eclipsed geometry. [d]PBE0/TZ2P, experimental eclipsed geometry.

Table S6: Calculated metal electronic configuration in vanadocene and nickelocene.[a]

System	Level	Spin	Configuration
$V(C_5H_5)_2$[b]	BP/TZ2P	α	$(3d_\sigma)^{0.96}(3d_\pi)^{0.74}(3d_\delta)^{1.77}$
		β	$(3d_\sigma)^{0.06}(3d_\pi)^{0.58}(3d_\delta)^{0.03}$
	PBE0/TZ2P	α	$(3d_\sigma)^{0.97}(3d_\pi)^{0.65}(3d_\delta)^{1.83}$
		β	$(3d_\sigma)^{0.06}(3d_\pi)^{0.50}(3d_\delta)^{0.02}$
$Ni(C_5H_5)_2$[b]	BP/TZ2P	α	$(3d_\sigma)^{0.99}(3d_\pi)^{1.99}(3d_\delta)^{1.94}$
		β	$(3d_\sigma)^{0.98}(3d_\pi)^{1.00}(3d_\delta)^{1.92}$
	PBE0/TZ2P	α	$(3d_\sigma)^{0.99}(3d_\pi)^{1.99}(3d_\delta)^{1.97}$
		β	$(3d_\sigma)^{0.99}(3d_\pi)^{0.76}(3d_\delta)^{1.95}$

[a]Natural population analyses. [b]The optimized D_{5h} geometry is used.

Table S7: Relative energies (in eV) between the lowest-lying spin-doublet electronic configurations of cobaltocene.[a]

Configuration[b]	CAS-SR / SO	PT2-SR / SO	Expt.[c]	Expt.[d]
$(\pi_+)^{3.90}(\sigma)^{1.97}(\delta_+)^{3.90}(\pi_-)^{1.13}$	*0.00 / 0.00*	*0.00 / 0.00*	0.00	0.00
	0.00 / 0.00	0.00 / 0.00		
	0.42 / 0.42	0.40 / 0.40		
$(\pi_+)^{3.92}(\sigma)^{1.65}(\delta_+)^{3.27}(\pi_-)^{2.07}$	*1.95 / 1.98*	*1.92 / 1.94*	1.88	1.90
	1.97 / 1.97	1.92 / 1.92		

[a]The energies given in italics are for the eclipsed BP/TZ2P geometry, otherwise the C_{2v} Jahn-Teller structure was used. [b] The π_+, σ, δ_+ and π_- notations are used for brevity instead of $(\pi_\pi - 3d_\pi)_+$, $3d_\sigma$, $(\pi_\delta - 3d_\delta)_+$ and $(\pi_\pi - 3d_\pi)_-$. Superscript numbers are occupations of the converged NOs at the eclipsed geometry. [c]From ref. 32, cobaltocene diluted in a ruthenocene single crystal at 4 K. [d]From ref 33, cobaltocene in isooctane solution.

Table S8: Relative energies (in eV) between the lowest-lying spin-quartet electronic configurations of vanadocene and spin-triplet ones of nickelocene.

System	Configuration[b]	CAS-SR(SO)	PT2-SR(SO)	Expt.[c]
$V(C_5H_5)_2$[a]	$(\pi_+)^{3.98}(\sigma)^{1.00}(\delta_+)^{1.98}(\pi_-)^{0.04}$	0.00 (0.00)	0.00 (0.00)	0.00
	$(\pi_+)^{3.99}(\sigma)^{0.23}(\delta_+)^{1.77}(\pi_-)^{1.01}$	1.93 (1.93)	2.22 (2.22)	2.14
$Ni(C_5H_5)_2$[a]	$(\pi_+)^{3.95}(\sigma)^{1.98}(\delta_+)^{3.93}(\pi_-)^{2.05}$	0.00 (0.00)	0.00 (0.00)	0.00
	$(\pi_+)^{3.98}(\sigma)^{1.24}(\delta_+)^{3.71}(\pi_-)^{2.99}$	1.79 (1.80)	1.73 (1.74)	1.80

[a]The eclipsed BP/TZ2P geometries are used. The CAS(7, 7) and CAS(12, 12) are used for vanadocene and nickelocene respectively. [b]The π_+, σ, δ_+ and π_- notations are used for brevity instead of $(\pi_\pi - 3d_\pi)_+$, $3d_\sigma$, $(\pi_\delta - 3d_\delta)_+$ and $(\pi_\pi - 3d_\pi)_-$. Superscript numbers are occupations of the converged NOs. [c]From ref. 33.

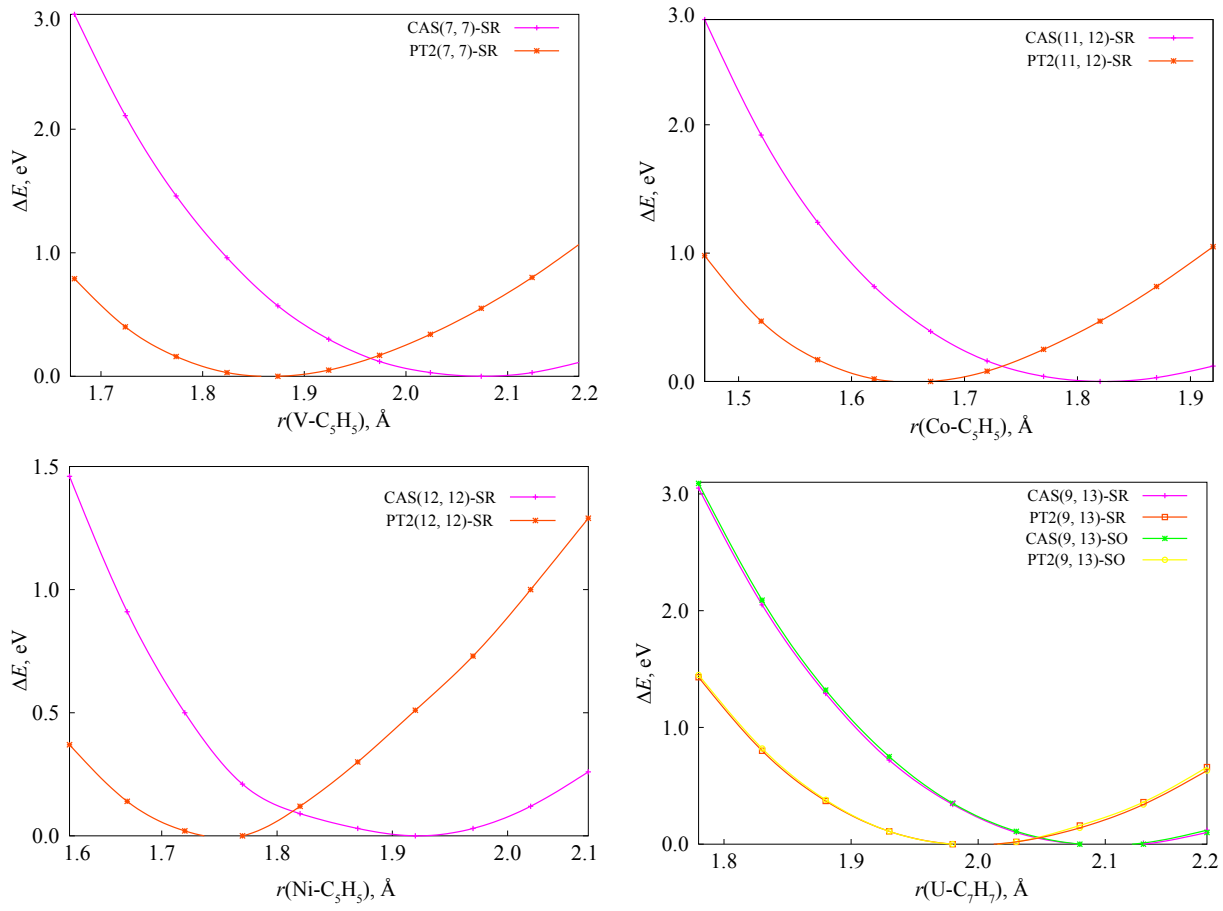

Figure S2: Evolution of the ground-state energy, calculated with different *ab initio* approaches, as a function of the distance between the metal center and ring centroids in the eclipsed BP/TZ2P structures of vanadocene (top left), cobaltocene (top right), nickelocene (bottom left), and in the eclipsed experimental structure of $U(C_7H_7)_2^-$ (bottom right).

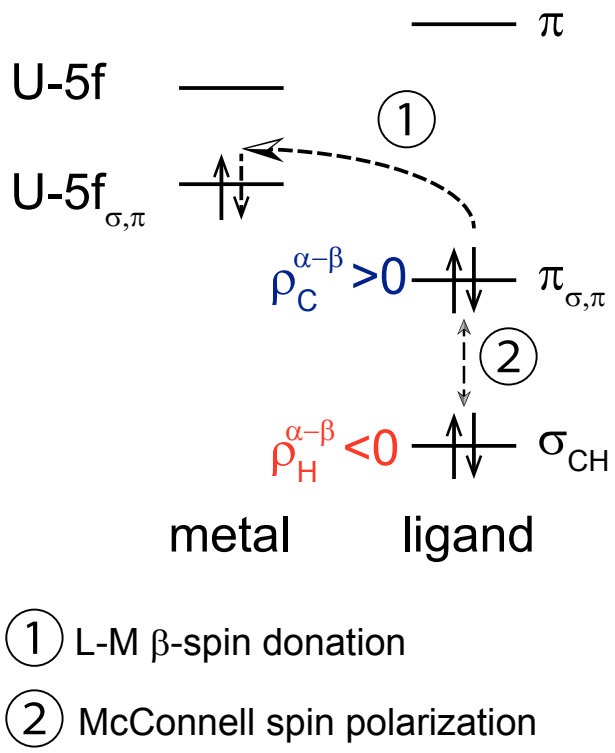

Figure S3: Simplified scheme, proposed by Gourier et al.[25] showing how a spin density in the $5f^1$ $U(C_7H_7)_2^-$ may arise at the arene C and H centers due to metal-ligand bonding.

Table S9: Excitation energies (in eV) between the SOC levels of the GS in V^{II+}, Co^{II+}, Ni^{II+} and U^{V+} ions obtained with CAS(3, 5)-SO, CAS(7, 5)-SO, CAS(8, 5)-SO and CAS(7, 15)-SO calculations respectively.[a]

Ion	Excitation	Calc.	Expt.[b]
V^{II+}	$^4F_{3/2} \rightarrow {}^4F_{5/2}$	0.019	0.018
	$^4F_{3/2} \rightarrow {}^4F_{7/2}$	0.047	0.042
	$^4F_{3/2} \rightarrow {}^4F_{9/2}$	0.083	0.072
Co^{II+}	$^4F_{9/2} \rightarrow {}^4F_{7/2}$	0.102	0.104
	$^4F_{9/2} \rightarrow {}^4F_{5/2}$	0.182	0.180
	$^4F_{9/2} \rightarrow {}^4F_{3/2}$	0.239	0.232
Ni^{II+}	$^3F_4 \rightarrow {}^3F_3$	0.164	0.169
	$^3F_4 \rightarrow {}^3F_3$	0.288	0.281
U^{IV+}	$^2F_{5/2} \rightarrow {}^4F_{7/2}$	0.982	0.943

[a]ANO-RCC-VTZP basis sets are used. For the TM ions, the active spaces comprise the five 3d orbitals and their electrons while the state average/state interaction spaces consist of 10 spin-quartet states for V and Co and 10 spin-triplet states for Ni. For the actinide ion, the CAS comprises the 5f, 6d and 6p orbitals and their electrons while the state average/state interaction spaces consist of 7 spin-doublet states. [b]From the NIST database.

Table S10: Low-lying electronic states for the $5f^1$ $U(C_7H_7)_2^-$: wavefunction compositions and relative energies obtained through CAS-SR /SO and PT2-SR / SO (values in parantheses).[a]

State	Composition[b]	ΔE(eV)	Composition[c]	ΔE(eV)
CAS(1, 7)-SR			CAS(1, 7)-SO[d]	
$^2\Sigma$	$(5f_\sigma)^{1.00}$	0.00 (0.00)	$70\%^2\Sigma+30\%^2\Pi$	0.00 (0.00)
$^2\Phi$	$(5f_\phi)^{1.00}$	0.29 (0.40)	$98\%^2\Phi$	0.15 (0.27)
$^2\Pi$	$(5f_\pi)^{1.00}$	0.53 (0.52)	$90\%^2\Pi+10\%^2\Delta$	0.81 (0.85)
$^2\Delta$	$(5f_\delta^-)^{1.00}$	1.91 (2.63)	$100\%^2\Phi$	0.92 (0.92)
			$70\%^2\Pi+30\%^2\Sigma$	0.93 (1.03)
			$90\%^2\Delta+10\%^2\Pi$	2.08 (2.76)
			$98\%^2\Delta+2\%^2\Phi$	2.43 (3.15)
CAS(5, 9)-SR			CAS(5, 9)-SO	
$^2\Sigma$	$(5f_\delta^+)^{3.73}(5f_\sigma)^{0.99}(5f_\delta^-)^{0.25}$	0.00 (0.00)	$70\%^2\Sigma+30\%^2\Pi$	0.00 (0.00)
$^2\Phi$	$(5f_\delta^+)^{3.74}(5f_\phi)^{0.99}(5f_\delta^-)^{0.25}$	0.32 (0.41)	$100\%^2\Phi$	0.33 (0.34)
$^2\Pi$	$(5f_\delta^+)^{3.71}(5f_\pi)^{0.98}(5f_\delta^-)^{0.24}$	0.51 (0.50)	$100\%^2\Pi$	0.93 (0.92)
^{2}LMCT	$(5f_\delta^+)^{2.97}(5f_\sigma)^{0.99}(5f_\phi)^{0.99}$	1.81 (1.72)	$70\%^2\Pi+30\%^2\Sigma$	0.95 (0.95)
			$100\%^2\Phi$	0.97 (1.06)
CAS(9, 16)-SR			CAS(9, 16)-SO	
$^2\Sigma$	$(6d_\delta^+)^{3.93}(5f_\delta^+)^{3.74}(5f_\sigma)^{0.99}(5f_\delta^-)^{0.24}$	0.00 (0.00)	$70\%^2\Sigma+30\%^2\Pi$	0.00 (0.00)
$^2\Phi$	$(6d_\delta^+)^{3.93}(5f_\delta^+)^{3.74}(5f_\phi)^{0.99}(5f_\delta^-)^{0.24}$	0.32 (0.38)	$98\%^2\Phi+2\%^2\Delta$	0.20 (0.27)
$^2\Pi$	$(6d_\delta^+)^{3.93}(5f_\delta^+)^{3.72}(5f_\pi)^{0.98}(5f_\delta^-)^{0.23}$	0.49 (0.47)	$92\%^2\Pi+8\%^2\Delta$	0.81 (0.79)
$^2\Delta$	$(6d_\delta^+)^{3.93}(5f_\delta^+)^{3.56}(5f_\delta^-)^{0.96}(5f_\phi)^{0.23}(5f_\pi)^{0.15}$	1.89 (1.84)	$70\%^2\Pi+30\%^2\Sigma$	0.92 (0.91)
			$100\%^2\Phi$	0.96 (1.03)
			$92\%^2\Delta+8\%^2\Pi$	2.12 (2.07)
			$98\%^2\Delta+2\%^2\Phi$	2.36 (2.32)

[a]The eclipsed experimental geometry is used. See Table S11 for results obtained at the eclipsed BP/TZ2P geometry. [b]The compositions of the SR wave functions are given in terms of the NOs that are significantly populated; the $6d_\delta^+$, $5f_\delta^+$ and $5f_\delta^-$ notations are used for brevity instead of $(\pi_\delta - 6d_\delta)_+$, $(\pi_\delta - 5f_\delta)_+$ and $(\pi_\delta - 5f_\delta)_-$. [c]Given in terms of the SR states on the first column.

Table S11: Calculated low-lying electronic states for the $5f^1$ $U(C_7H_7)_2^-$: wave function compositions and relative energies obtained through CAS-SR / SO and PT2-SR / SO (values listed parenthesis).[a]

State	Composition[b]	ΔE(eV)	Composition[c]	ΔE(eV)
CAS(1, 7)-SR			CAS(1, 7)-SO	
$^2\Sigma$	$(5f_\sigma)^{1.00}$	0.00 (0.00)	$68\%^2\Sigma+32\%^2\Pi$	0.00 (0.00)
$^2\Phi$	$(5f_\phi)^{1.00}$	0.26 (0.35)	$98\%^2\Phi$	0.14 (0.24)
$^2\Pi$	$(5f_\pi)^{1.00}$	0.47 (0.45)	$96\%^2\Pi+4\%^2\Delta$	0.76 (0.80)
$^2\Delta$	$(5f_\delta^-)^{1.00}$	1.75 (2.48)	$100\%^2\Phi$	0.91 (0.91)
			$68\%^2\Pi+32\%^2\Sigma$	0.92 (1.01)
			$96\%^2\Delta+4\%^2\Pi$	1.95 (2.63)
			$98\%^2\Delta+2\%^2\Phi$	2.30 (3.02)
CAS(5, 9)-SR			CAS(5, 9)-SO	
$^2\Sigma$	$(5f_\delta^+)^{3.70}(5f_\sigma)^{0.99}(5f_\delta^-)^{0.28}$	0.00 (0.00)	$67\%^2\Sigma+33\%^2\Pi$	0.00 (0.00)
$^2\Phi$	$(5f_\delta^+)^{3.70}(5f_\phi)^{0.98}(5f_\delta^-)^{0.28}$	0.29 (0.36)	$100\%^2\Phi$	0.24 (0.31)
$^2\Pi$	$(5f_\delta^+)^{3.67}(5f_\pi)^{0.98}(5f_\delta^-)^{0.27}$	0.46 (0.43)	$100\%^2\Pi$	0.89 (0.88)
^{2}LMCT	$(5f_\delta^+)^{2.97}(5f_\sigma)^{0.98}(5f_\phi)^{0.98}$	1.67 (1.55)	$67\%^2\Pi+33\%^2\Sigma$	0.94 (0.94)
			$100\%^2\Phi$	0.96 (1.04)
CAS(9, 13)-SR			CAS(9, 13)-SO	
$^2\Sigma$	$(6d_\delta^+)^{3.94}(5f_\delta^+)^{3.71}(5f_\sigma)^{0.99}(5f_\delta^-)^{0.27}$	0.00 (0.00)	$67\%^2\Sigma+33\%^2\Pi$	0.00 (0.00)
$^2\Phi$	$(6d_\delta^+)^{3.94}(5f_\delta^+)^{3.71}(5f_\phi)^{0.99}(5f_\delta^-)^{0.28}$	0.26 (0.35)	$98\%^2\Phi+2\%^2\Delta$	0.16 (0.26)
$^2\Pi$	$(6d_\delta^+)^{3.94}(5f_\delta^+)^{3.68}(5f_\pi)^{0.98}(5f_\delta^-)^{0.26}$	0.45 (0.40)	$92\%^2\Pi+8\%^2\Delta$	0.78 (0.74)
$^2\Delta$	$(6d_\delta^+)^{3.94}(5f_\delta^+)^{3.52}(5f_\delta^-)^{0.97}(5f_\phi)^{0.18}(5f_\pi)^{0.26}$	1.78 (1.64)	$67\%^2\Pi+33\%^2\Sigma$	0.92 (0.91)
			$100\%^2\Phi$	0.93 (1.05)
			$92\%^2\Delta+8\%^2\Pi$	2.03 (1.92)
			$98\%^2\Delta+2\%^2\Phi$	2.27 (2.15)
CAS(9, 16)-SO			CAS(9, 16)-SO	
$^2\Sigma$	$(6d_\delta^+)^{3.93}(5f_\delta^+)^{3.71}(5f_\sigma)^{0.98}(5f_\delta^-)^{0.27}$	0.00 (0.00)	$67\%^2\Sigma+33\%^2\Pi$	0.00 (0.00)
$^2\Phi$	$(6d_\delta^+)^{3.93}(5f_\delta^+)^{3.70}(5f_\phi)^{0.98}(5f_\delta^-)^{0.28}$	0.29 (0.34)	$98\%^2\Phi+2\%^2\Delta$	0.19 (0.25)
$^2\Pi$	$(6d_\delta^+)^{3.92}(5f_\delta^+)^{3.68}(5f_\pi)^{0.98}(5f_\delta^-)^{0.26}$	0.43 (0.40)	$92\%^2\Pi+8\%^2\Delta$	0.76 (0.78)
$^2\Delta$	$(6d_\delta^+)^{3.92}(5f_\delta^+)^{3.52}(5f_\delta^-)^{0.96}(5f_\phi)^{0.25}(5f_\pi)^{0.18}$	1.71 (1.65)	$67\%^2\Pi+33\%^2\Sigma$	0.91 (0.90)
			$100\%^2\Phi$	0.96 (1.00)
			$92\%^2\Delta+8\%^2\Pi$	1.97 (1.91)
			$98\%^2\Delta+2\%^2\Phi$	2.21 (2.16)

[a]The SR eclipsed BP/TZ2P geometry is used, [b]The compositions of the SR wave functions are given in terms of the active-space NO that are significantly populated; the $6d_\delta^+$, $5f_\delta^+$ and $5f_\delta^-$ notations are used for brevity instead of $(\pi_\delta - 6d_\delta)_+$, $(\pi_\delta - 5f_\delta)_+$ and $(\pi_\delta - 5f_\delta)_-$. [c]SOC wave-function composition given in terms of the SR states printed on the first column.

Table S12: Calculated lowest-lying electronic states for the $5f^1$ $U(C_7H_7)_2^-$ complex:[a] wave-function compositions and relative energies obtained through CAS-SR / SO approaches.[b]

State	Composition[c]	ΔE	Composition[d]	ΔE
CAS(5, 9)-SR			CAS(5, 9)-SO	
$^2\Sigma$	$(5f_\delta^+)^{3.71}(5f_\sigma)^{0.98}(5f_\delta^-)^{0.25}$	0.00	70%$^2\Sigma$+30%$^2\Pi$	0.00
$^2\Phi$	$(5f_\delta^+)^{3.66}(5f_\phi)^{0.97}(5f_\delta^-)^{0.24}$	0.37	100%$^2\Phi$	0.29
$^2\Pi$	$(5f_\delta^+)^{3.62}(5f_\pi)^{0.95}(5f_\delta^-)^{0.21}$	0.51	100%$^2\Pi$	0.91
^{2}LMCT	$(5f_\delta^+)^{2.91}(5f_\sigma)^{0.97}(5f_\phi)^{0.97}$	1.90	70%$^2\Pi$+30%$^2\Sigma$	0.92
			100%$^2\Phi$	0.98
			100%^{2}LMCT	1.97

[a]The eclipsed experimental geometry is used, [b]The ORCA4.0 software package[34] is used to perform these calculations; the segmented all-electrons relativistically contracted valence triple-ζ (SARC-TZVP) basis set[35] is used for the U center while the def2-TZVP ones[36,37] are used for C and H centers; SR effects are introduced through the second-order Douglass-Kroll-Hess (DKH2) Hamiltonian.;[38–40] SOC is introduced through the mean-field spin-orbit configuration interaction approach as implemented in ORCA, [c]The compositions of the SR wave functions are given in terms of the NOs that are significantly populated; the $5f_\delta^+$ and $5f_\delta^-$ notations are used for brevity instead of$(\pi_\delta - 5f_\delta)_+$ and $(\pi_\delta - 5f_\delta)_-$. [d]Given in terms of the SR states shown on the left column.

Table S13: Expectation values of the spin and angular momentum obtained for the GS of the $5f^1$ $U(C_7H_7)_2^-$ system through CAS-SO calculations.

Active space	$\langle L_\parallel \rangle$	$\langle L_\perp \rangle$	$\langle S_\parallel \rangle$	$\langle S_\perp \rangle$
CAS(1, 7)	$\pm$0.283	$\pm$1.498	$\pm$0.211	$\mp$0.356
CAS(5, 9)	$\pm$0.297	$\pm$1.845	$\pm$0.197	$\mp$0.348
CAS(9, 13)	$\pm$0.298	$\pm$1.895	$\pm$0.197	$\mp$0.348
CAS(9, 16)	$\pm$0.299	$\pm$1.781	$\pm$0.196	$\mp$0.348

[a]The eclipsed experimental geometry is used.

Table S14: Calculated GS g factors for vanadocene and nickelocene.[a]

Functional	Approach	$V(C_5H_5)_2$			$Ni(C_5H_5)_2$		
		g_1	g_2	g_3	g_1	g_2	g_3
BP	SR-ZORA[b]	2.00	2.00	2.00	2.00	2.04	2.04
	SO-ZORA[c]	1.99	1.99	2.00	2.00	2.04	2.04
PBE	SR-ZORA[b]	2.00	2.00	2.00	2.00	2.04	2.04
	SO-ZORA[c]	2.00	2.00	2.00	2.00	2.04	2.04
B3LYP	SR-ZORA[b]	1.99	1.99	2.00	2.00	2.09	2.09
	SO-ZORA[c]	1.99	1.99	2.00	2.00	2.08	2.08
PBE0	SR-ZORA[b]	1.99	1.99	2.00	2.00	2.09	2.09
	SO-ZORA[c]	1.99	1.99	2.00	2.00	2.08	2.08
-	CAS-SO[d]	1.98	1.98	2.00	2.00	2.14	1.14
-	PT-SO[d]	1.98	1.98	2.00	2.00	2.14	2.14
Expt.[e]		1.99	1.99	2.00	2.00	2.11	2.11

[a]The SR eclipsed geometries are used. [b]Perturbative treatment of SOC. [c]Spin-unrestricted calculations using the collinear approach. [d]The CAS(7, 7) and CAS(12, 12) are used for vanadocene and nickelocene respectively. [e]Data from ref. 41 for vanadocene and from ref. 42 for nickelocene.

Table S15: Calculated GS g factors for $U(C_7H_7)_2^-$ with CAS-SO and PT2-SO using various active spaces.[a]

Method	$g_\parallel$	$g_\perp$
CAS(1, 7)-SO	1.41	1.57
PT(1, 7)-SO	1.41	1.59
CAS(5, 9)-SO	1.38	2.29
PT(5, 9)-SO	1.38	2.30
CAS(9, 16)-SO	1.38	2.17
PT2(9, 16)-SO	1.36	2.23
Expt.[b]	1.24	2.37

[a]The eclipsed experimental geometry is used for the $5f^1$ $U(C_7H_7)_2^-$. [b]Data from ref. 25.

Table S16: Calculated GS isotropic HyFCCs (in MHz) for vanadocene and nickelocene.[a]

Functional	Approach	$V(C_5H_5)_2$		$Ni(C_5H_5)_2$	
		$A_{iso}^{^{13}C}$	$A_{iso}^{^{1}H}$	$A_{iso}^{^{13}C}$	$A_{iso}^{^{1}H}$
BP	SR-ZORA	−0.88	3.01	3.96	−4.36
	SR-ZORA[b]	−0.85	3.02	3.81	−4.39
	SO-ZORA[c]	−0.78	3.01	3.74	−4.38
PBE	SR-ZORA	−0.89	3.08	4.47	−4.10
	SR-ZORA[b]	−0.87	3.08	4.32	−4.14
	SO-ZORA[c]	−0.80	3.09	4.32	−4.13
B3LYP	SR-ZORA	−0.60	2.61	4.83	−3.67
	SR-ZORA[b]	−0.57	2.62	4.64	−3.71
	SO-ZORA[c]	−0.53	2.61	4.64	−3.72
PBE0	SR-ZORA	−1.10	2.80	5.10	−3.71
	SR-ZORA[b]	−1.07	2.81	4.91	−3.77
	SO-ZORA[c]	−1.02	2.81	4.91	−3.75
Expt.[d]		-	2.33	-	−3.53

[a]GS data. The eclipsed geometries are used. [b]Perturbative treatment of SOC. [c]Spin-unrestricted calculations using the collinear approach. [d]Data from ref. 43 for both vanadocene and nickelocene.

References

[1] A. K. Hedberg, L. Hedberg and K. Hedberg, *J. Chem. Phys.*, 1975, **63**, 1262–1266.

[2] A. Almenningen, E. Gard, A. Haaland and J. Brunvoll, *J. Organomet. Chem.*, 1976, **107**, 273–279.

[3] E. Gard, A. Haaland, D. P. Novak and R. Seip, *J. Organomet. Chem.*, 1975, **88**, 181–189.

[4] L. Hedberg and K. Hedberg, *J. Chem. Phys.*, 1970, **53**, 1228–1234.

[5] M. Y. Antipin, R. Boese, N. Augart and G. Schmid, *Struct. Chem.*, 1993, **4**, 91–101.

[6] P. Seiler and J. D. Dunitz, *Acta Cryst.*, 1980, **B36**, 2255–2260.

[7] R. D. Rogers, J. L. Atwood, D. Foust and M. D. Rausch, *J. Cryst. Mol. Struct.*, 1981, **11**, 183–188.

[8] T. A. Jackson, J. Krzystek, A. Ozarowski, G. B. Wijeratne, B. F. Wicker, D. J. Mindiola and J. Telser, *Organometallics*, 2012, **31**, 8265–8274.

[9] T. Arliguie, M. Lance, M. Nierlich, J. Vigner and M. Ephritikhine, *J. Chem. Soc., Chem. Commun.*, 1995, 183–184.

[10] M. Swart and J. G. Snijders, *J. Theor. Chem. Acc.*, 2003, **110**, 34–41.

[11] M. Swart, *Inorg. Chim. Acta.*, 2006, **360**, 179–189.

[12] S. Coriani, A. Haaland, T. Helgaker and P. Jørgensen, *ChemPhysChem*, 2006, **7**, 245–249.

[13] H. Koch, P. Jørgensen and T. Helgaker, *J. Chem. Phys.*, 1996, **104**, 9528–9530.

[14] Z.-F. Xu, Y. Xie, W.-L. Feng and H. F. Schaefer, *J. Phys. Chem.* **A**, 2003, **107**, 2716–2729.

[15] Q. M. Phung, S. Vancoillie and K. Pierloot, *J. Chem. Theory Comput.*, 2012, **8**, 883–892.

[16] E. Solis-Cèspedes and D. Páez-Hernández, *Dalton Trans.*, 2017, **46**, 4834–4843.

[17] P. Hrobárik, R. Reviakine, A. V. Arbuznikov, O. L. Malkina, V. G. Malkin, F. H. Köhler and M. Kaupp, *J. Chem. Phys.*, 2007, **126**, 024107–19.

[18] K. Pierloot, B. J. Persson and B. O. Roos, *J. Phys. Chem.*, 1995, **99**, 3465–3472.

[19] J. Li and B. E. Bursten, *J. Am. Chem. Soc.*, 1997, **119**, 9021–9032.

[20] H. A. Jahn and E. Teller, *Proc. R. Soc. Lond. A*, 1937, **161**, 220–235.

[21] I. B. Bersuker, *Chem. Rev.*, 2001, **101**, 1067–1114.

[22] K. Andersson and B. O. Roos, *Chem. Phys. Lett.*, 1992, **191**, 507–514.

[23] Q. M. Phung, S. Vancoillie and K. Pierloot, *J. Chem. Theory Comput.*, 2014, **10**, 3681–3688.

[24] C. J. Stein, V. von Burg and M. Reiher, *J. Chem. Theory Comput.*, 2016, **12**, 3764–3773.

[25] D. Gourier, D. Caurant, T. Arliguie and M. Ephritikhine, *J. Am. Chem. Soc.*, 1998, **120**, 6084–6092.

[26] F. Gendron, D. Páez-Hernández, F.-P. Notter, B. Pritchard, H. Bolvin and J. Autschbach, *Chem. Eur. J.*, 2014, **20**, 7994–8011.

[27] A. Kerridge and N. Kaltsoyannis, *J. Phys. Chem. A*, 2009, **113**, 8737–8745.

[28] W. Liu, M. Dolg and P. Fulde, *J. Chem. Phys.*, 1997, **107**, 3584–3591.

[29] A. H. H. Chang and R. M. Pitzer, *J. Am. Chem. Soc.*, 1989, **111**, 2500–2507.

[30] A. Avdeef, K. N. Raymond, K. O. Hodgson and A. Zalkin, *Inorg. Chem.*, 1972, **11**, 1083–1088.

[31] D. Seyferth, *Organometallics*, 2004, **23**, 3562–3583.

[32] J. Weber, A. Goursot, E. Pénigault, J. H. Ammeter and J. Bachmann, *J. Am. Chem. Soc.*, 1982, **104**, 1491–1506.

[33] K. R. Gordon and K. D. Warren, *Inorg. Chem.*, 1978, **17**, 987–994.

[34] F. Neese, *ORCA – An Ab initio, DFT and Semiempirical SCF-MO Package, Version 4.0, Max-Planck-Institute for Chemical Energy Conversion, Mülheim an der Ruhr, Germany; available from* `https://orcaforum.cec.mpg.de`, 2017.

[35] D. A. Pantazis and F. Neese, *J. Chem. Theory Comput.*, 2011, **7**, 677–684.

[36] F. Weigend and R. Ahlrichs, *Phys. Chem. Chem. Phys.*, 2005, **7**, 3295–3305.

[37] F. Weigend, *Phys. Chem. Chem. Phys.*, 2006, **8**, 1057–1065.

[38] M. Douglas and N. M. Kroll, *Ann. Phys.*, 1974, **82**, 89–155.

[39] B. A. Hess, *Phys. Rev. A*, 1985, **32**, 756–763.

[40] B. A. Hess, *Phys. Rev. A*, 1986, **33**, 3742–3748.

[41] S. Li, Y. Hamrick, R. Van Zee and W. Weltner Jr, *J. Am. Chem. Soc.*, 1992, **114**, 4433–4434.

[42] P. Baltzer, A. Furrer, J. Hulliger and A. Stebler, *Inorg. Chem.*, 1988, **27**, 1543–1548.

[43] M. F. Rettig and R. S. Drago, *J. Am. Chem. Soc.*, 1969, **91**, 1361–1370.